Proceedings of the ASME 2018 37th International Conference on Ocean, Offshore and Arctic Engineering
OMAE2018
June 17-22, 2018, Madrid, Spain

OMAE2018-77254

NUMERICAL AND EXPERIMENTAL STUDY ON THE SEAKEEPING BEHAVIOR OF FLOATING CLOSED RIGID FISH CAGES

David Kristiansen *
SINTEF Ocean
Trondheim, Norway
Email: david.kristiansen@sintef.no

Pål Lader
Norwegian University of Science and Technology (NTNU)
Trondheim, Norway

Per C. Endresen
SINTEF Ocean
Trondheim, Norway

Vegard Aksnes
SINTEF Ocean
Trondheim, Norway

ABSTRACT

The present paper addresses the seakeeping behavior of a rigid type of floating closed fish cages, with focus on effects of sloshing on the coupled motions and mooring loads. Closed cages have gained much attention recently as a strategy to avoid sea-lice infections in farming of Atlantic salmon. However, closed cages are novel structures and more knowledge is needed on the wave induced motions and coupling effects with sloshing for development of reliable closed cage structures to reduce risk for failure and possible escape of fish. In this paper, dedicated scaled model tests of closed cages in waves are presented and compared with numerical simulations using linear potential theory in frequency domain. The results shows that the influence of sloshing on the rigid body motion is significant. A nonlinear effect of sloshing was observed for a small region of excitation frequencies, where the surge amplitude increased with increasing wave steepness. Mean wave loads were also affected by sloshing. Hence, coupled motions with sloshing is important to consider in design of floating closed rigid fish cages and their mooring system.

*Address all correspondence to this author.

INTRODUCTION

This paper addresses the seakeeping behaviour and mooring forces of floating closed containment systems for fish farming, when exposed to waves. Attention is put on sloshing of the contained water and associated coupling effects on the wave induced rigid body motions of the structure. Floating closed containment systems, hereafter referred to as closed cages, have gained increased interest among Norwegian fish farmers in recent years in order to improve the on-growth stage for sea-based production of Atlantic salmon (*Salmo salar*). Traditionally, farming of Atlantic salmon is performed in floating net cages, where exchange of water inside the cage are due to natural convection from the surrounding water. A major challenge for the traditional production is the problem of sea-lice infections, caused by contaminated water from the environment. Due to high stocking densities within the farm, sea-lice infections may cause further contamination of the water with subsequent infection of nearby salmonid fish stocks, farmed or wild. By use of closed cages which separates the water volume for production from the surrounding water, except for a controlled system for water exchange, it is possible to minimize the risk for sea-lice infections, optimize water quality for salmon production and to reduce the impact on the local environment by collection of waste. The use of closed

cages in Norwegian aquaculture is still limited and closed cages are typically installed at sheltered fjord locations. Hence, there is limited experience on the behavior of closed cages in waves, but some incidents have been reported with structural damages in bad weather. On the other hand, several new closed cage concepts have recently been proposed by the salmon farming industry in Norway, some pointing to more weather exposed locations. There is a need for more knowledge on the seakeeping behavior of closed cage structures to ensure the development of reliable structures and reduce the risk for damages and possible fish escapes.

A floating closed cage can be described as a floating tank structure with an internal free-surface. Several different concepts exist with various geometric shapes, structural properties and engineering materials being used. It is convenient to categorize closed cage structure concepts into 1) rigid structures, 2) elastic structures and 3) flexible membrane structures. The difference of structural properties between these three categories suggest different seakeeping behavior and also different required modeling approaches. Design aspects of closed flexible cages of the third category was studied by [1]. These are typically made of coated fabric and the flexible nature of these structures implies that hydroelasticity is important to consider when responses to hydrodynamic loading from the marine environment are analyzed [2]. A study of drag force and associated deformations of closed flexible cages from scaled model experiments was presented in [3] and [4], followed up by an experimental study on the wave induced responses of the same closed flexible structure [5]. To the authors best knowledge, there are no previous works published on the seakeeping behavior of closed cage structures of the rigid and elastic type (category 1 and 2). However, studies on sloshing and the coupled motions of ships are highly relevant. Sloshing, or resonant liquid motion in a tank with a free surface, is a complex phenomenon with relevance for many applications [6]. A study of the effect of sloshing on ship motions was presented by [7], where liquid sloshing motions measured in 2D experiments were shown to compare well with numerical estimates using the nonlinear multi-modal theory by [8]. Nonlinear analyses of coupled ship motions and sloshing were also presented by [9] and [10]. Linear potential flow theory has also been used to study coupling of ship motions and sloshing, both in frequency domain [11] and in time domain [12].

In the present paper, scaled physical experiments of a floating closed-cage model in waves are presented. Two model configurations were tested to investigate the coupling effects of the contained water on the rigid body motions; One configuration where the model was filled with water, and one where the contained water was replaced by fixed weights. Both model configurations were moored and tested in regular waves. Measured responses from the experiments were compared with numerical estimates from linear potential flow theory in frequency domain using WAMIT.

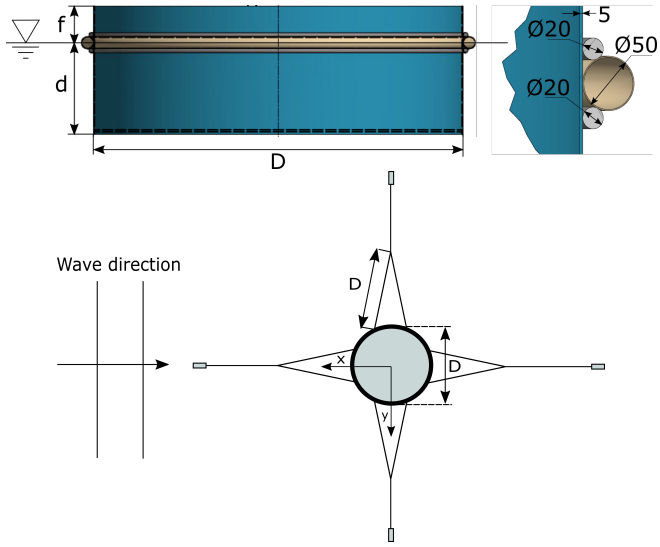

FIGURE 1: SKETCH OF MODEL GEOMETRY AND SETUP. TOP: SIDE VIEW (LEFT). DETAIL OF FLOATING COLLAR WITH MEASURES IN mm (RIGHT). BOTTOM: TOP VIEW OF MODEL SETUP WITH MOORINGS.

MATERIAL AND METHODS

Scaled Physical Model Tests

Physical model tests of scaled floating closed containments were conducted in a wave tank at SINTEF Ocean, Trondheim Norway, in March 2017. The wave tank is 10.5 m wide, 10 m deep and 85 m long, and equipped with a double flap type wavemaker and a parabolic beach.

The models A generic floating closed cage structure of the rigid type was designed for the model experiments with a chosen model scale 1:27. The model geometry was a circular cylinder with depth h=0.375 m and outer diameter D=1.50 m. The side wall of the cylindrical cage were made of 5 mm sheets of polycarbonate resin (Lexan). Hence, the internal diameter of the tank was 1.49 m. The flat bottom was a two layer construction with a sheet of the expanded PVC-based material Divinycell below and a sheet of compact PVC on top, both having a thickness of 10 mm. To ensure sufficient stability and buoyancy, a torus shaped floating collar was attached to the outsize of the cylindrical cage, centered in the design mean water line. The floating collar was constructed of plastic electrical tube with diameter 0.050 m. For additional stiffness of the cage in the mean water line, two massive aluminum rings with a cross-section diameter of 20 mm were added above and below the floating collar (cf. Fig. 1). The freeboard of the model was 0.15 m from the mean water line to the top rim of the model. To avoid water coming into the cage due to wave run-up at the front, a splashguard was mounted on the top rim at the side of the cage directed to-

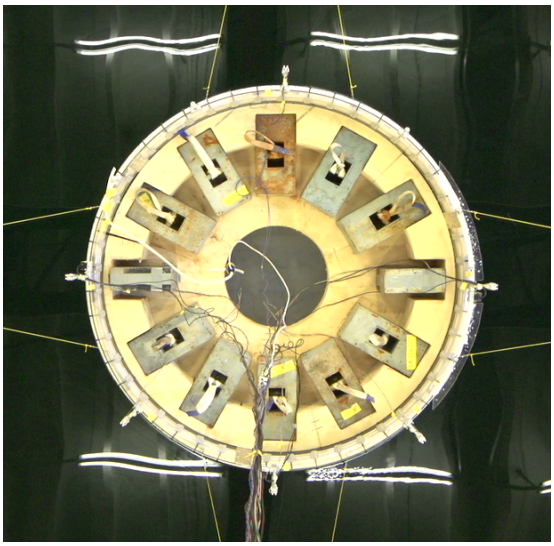

FIGURE 2: THE DRY MODEL CONFIGURATION WITH DISTRIBUTED WEIGHTS TO RESEMBLE FROZEN WATER.

wards the wavemaker. The eight bridle lines of the mooring were attached to eye-bolts in the top aluminum ring, evenly distributed along the circumference of the collar.

Two model configurations were tested. A *wet* model configuration where the closed cage was filled with water up to the design mean water line. Water was pumped into the cage from the wave tank. A second *dry* model configuration where the contained water was replaced by fixed weights, distributed to resemble frozen water (see Fig. 2). The main properties of the wet and dry model configurations are given in Tab. 1. The contained water is not included in given the mass and pitch gyration radius for the wet model configuration, where the latter is estimated numerically. Quasi-static effect of internal free surface is included in the predicted metacentric height for the wet model.

Instrumentation and setup The model was moored with four mooring lines in the water plane, two in-line with the incident wave propagation direction and two in the transverse direction (see Fig. 1). Two bridles where connected to each mooring line, providing in total eight mooring attachments on the model. The attachment points were equally spaced along the perimeter of the model at the mean water-line. The length of the bridle lines were equal to the cage diameter, i.e. 1.5 m. A multi-filament line with high stiffness was used for the moorings and bridles. Each of the four mooring lines were directed upwards from the water plane by means of a pulley and attached to coil springs to model the elastic effects of the mooring system. The pulleys were elevated 0.30 m above the calm water surface to avoid contact with water and disturbance of waves during

TABLE 1: STRUCTURAL PARAMETERS OF THE WET AND DRY MODEL CONFIGURATIONS FROM THE EXPERIMENTS, WITH VALUES IN MODEL SCALE.

Parameter	Symbol	Dry model Value	Wet model Value
Diameter	D	1.5 m	1.5 m
Draft	d	0.375 m	0.375 m
Freeboard	f	0.15 m	0.15 m
Dry mass	M	666.3 kg	48.55 kg
Vert. centre of gravity	VCG	-0.186 m	-0.223 m
Pitch gyration radius	r_{55}	0.302 D	0.330 D
Metacentric height	GM	0.48 m	0.16 m

the tests. Due to this, the mooring lines made an angle of $\sim 5^\circ$ relative to the calm water surface. Coil springs with stiffness $k = 90$ N/m were applied for each mooring line, yielding an in-line equivalent horizontal stiffness of 180 N/m for the system. The yield limit of the springs were 120 N per mooring line. Tension in each mooring line was measured by a uni-axial load-cell that connected the mooring line to the spring. A pretension of 40 N was applied to all mooring lines.

Rigid body motions were obtained with an optical system (Qualisys Oqus), where the position of markers mounted on the model was tracked from camera images by use of triangularization. The translatory motion $\mathbf{s}_i$ of the i-th marker was related to the rigid body motions of the cage model by the linearized equation $\mathbf{s}_i = \eta + \omega \times \mathbf{r}_i$, where η and ω are the three dimensional vectors of translatory and rotational modes of motion, respectively, while $\mathbf{r}_i$ is the position vector of the i-th marker relative to the origin. Eight markers (reflectors) were distributed along the perimeter of the cage models with an elevation of 0.235 m above the mean water line, such that also eventual flexible deformations of the cage could be detected. Induced accelerations of the model were measured by three accelerometers mounted on the cage collar at angles $[0^\circ, 90^\circ, 180^\circ]$ along the perimeter, where 0° is on the longitudinal ($x-$) axis on the wavemaker side of the model. The capacity of the accelerometers was $2g$. Wave elevation in the wave tank exterior to the model was measured at three locations by conventional wave probes. Sloshing of the contained water inside the cage model was measured by use of conductive tape glued onto the wall at six different locations along the cage perimeter. This means that wave run-up on the tank wall was measured in a body-fixed reference frame. All data acquisition was performed with a sampling frequency of 200 Hz.

Test Conditions Each model was tested in regular waves defined by 23 wave periods and three wave steepnesses. The wave periods were in the range between 0.69 s and 2.50 s, corresponding to relative wavelengths λ/D in the range from 0.49 to 6.4, and the input steepnesses were $H/\lambda = [1/60, 1/45, 1/30]$. All tests with the water-filled (wet) model configuration was performed with 100 % fill ratio, such that the water level inside the model was approximately level with the exterior mean free surface.

Decay tests Free decay tests were performed in surge, heave and pitch for both model configurations, to estimate the damping ratios and the natural periods of the free motions. The tests were started by giving the model a perturbation from equilibrium in the considered mode of motion, trying to minimize the coupling to other degrees of freedom. The model was held at the perturbed position until the model and surrounding water were come to rest, before the model was released and started free decay motions back to equilibrium. Mooring line tensions, body motions and accelerations were measured during the tests.

Signal Processing

Measurement time-series were analyzed to obtain steady state wave responses. For each test, a time window was extracted where the wave induced motions were considered to have reached a steady state. The start time of this window was for each test obtained by estimating the time instant when the wave front for the considered regular wave has reached the model position, according to linear wave theory. The length of the time window was 20 wave periods. To reduce end-effects of the extracted time window during spectral analysis of the time series, the time series was tapered at both ends by means of a Bingham window (see [13], p. 146). All signals were band-pass filtered by multiplication of a Gaussian mask to the signals frequency spectrum obtained by Fourier transform (FFT). The measured motions of the Oqus markers of the optical motion tracking system can be erroneous for a limited time interval due to incorrect interpretation or fall-out of reflection signals. This would result in biased errors in the deduced rigid body motions, if not accounted for. Hence, the position measurements were post-processed to reject eventual outliers. The outliers were detected based on the *median absolute deviation* (MAD) algorithm (see e.g. [14]), where $\text{MAD} = median(|X_i - median(\mathbf{X})|)$ is the median absolute deviation of the sample X_i from the data-set $\mathbf{X}$. Then outliers X_i^{out} were defined as the sample offsets from the median of the time-series that exceeded a given threshold k, i.e. where $|X_i - median(\mathbf{X})| > k\text{MAD}$. The threshold value $k = 3$ was used in the present analysis, and the detected outliers were replaced by $median(\mathbf{X})$. The motions of the markers $\mathbf{s}_1$ at the front and $\mathbf{s}_5$ at the aft of the model, where $\mathbf{s}_i = [x_i, y_i, z_i]$, were used to detect the rigid body motions in surge (η_1), heave (η_3) and pitch (η_5) of the cage model from the following relations:

$$\eta_3 = \frac{z_1 + z_5}{2}, \quad \eta_5 = \frac{z_1 - z_5}{D}, \quad \eta_1 = \frac{x_1 + x_5}{2} + h\eta_5 \qquad (1)$$

where D is the cage diameter and h is the vertical position of the markers relative to the mean water line outside the model.

Sloshing Modes

According to linear potential flow theory, the velocity potential of liquid motion inside an upright circular cylindrical tank can be expressed as [6]

$$\varphi_{m,n}(r,\theta,z) = J_m\left(l_{m,n}\frac{r}{R_0}\right)\frac{\cosh(l_{m,n}(z+h)/R_0)}{\cosh(l_{m,n}h/R_0)} \times \begin{cases} \cos(m\theta) \\ \sin(m\theta) \end{cases}, \quad m = 0,1,...; \quad n = 1,2,.... \qquad (2)$$

where J_m is the Bessel function of the first kind of order m, R_0 is the tank radius and h is the tank water depth. Further, $l_{m,n}$ are the non-dimensional roots of the equation $J'_m(l_{m,n}) = 0$, which corresponds to waves with zero radial velocity at the wall boundary. The surface wave patterns of the normal modes are then found as $f_{m,n}(r,\theta) = \varphi_{m,n}(r,\theta,0)$. The natural periods corresponding to the different sloshing modes are found from

$$T_{m,n} = \frac{2\pi}{\sqrt{g l_{m,n}\tanh(l_{m,n}h/R_0)/R_0}} \qquad (3)$$

The first six sloshing mode shapes and associated natural periods in model scale are presented in Fig. 3.

Numerical Model

The closed cage was modeled in WAMIT [15] as a moored floating body in water of infinite depth and with a free surface without bounds. The geometry of the physical model was discretized by a grid of quadrilateral elements, but where the geometrical representation of the floating collar was simplified to avoid numerical problems (cf. Fig. 4 and 1). Simplifications of the geometry representation were made such that the water-plane area and the displacement of the cage was conserved. The base case grid for the dry model consisted of 3360 panels, while for the wet model where the inside tank was included, consisted of 6360 panels. The low-order method was used, where the solution of the potential is approximated by piecewise constant values on each panel. A liquid tank utility of the software was applied to model the coupled effects of the liquid motions of the contained water volume and the rigid body motions of the closed cage. The mooring was modeled as linear restoring forces with effective spring constants from the physical experiments, i.e. with

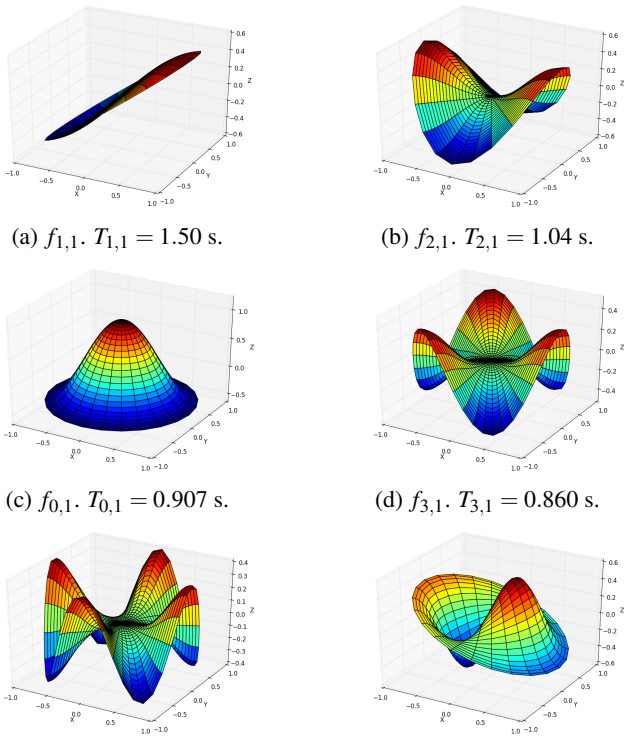

(a) $f_{1,1}$. $T_{1,1} = 1.50$ s. (b) $f_{2,1}$. $T_{2,1} = 1.04$ s.

(c) $f_{0,1}$. $T_{0,1} = 0.907$ s. (d) $f_{3,1}$. $T_{3,1} = 0.860$ s.

(e) $f_{4,1}$. $T_{4,1} = 0.757$ s. (f) $f_{1,2}$. $T_{1,2} = 0.756$ s.

FIGURE 3: Surface wave pattern of first sloshing modes and corresponding natural periods in model scale.

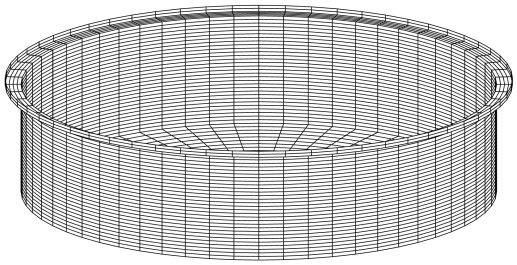

FIGURE 4: Mesh of quadrilateral elements used in numerical calculations with WAMIT.

$c_{11} = 180$ N/m. Pretension in the mooring lines yielded a pitch restoring moment with $c_{55} = F_0 D$, where $F_0 = 40$ N is the measured pretension in the experiments and D is the cage diameter. Response amplitude operators (RAO's) in surge, heave and pitch were calculated.

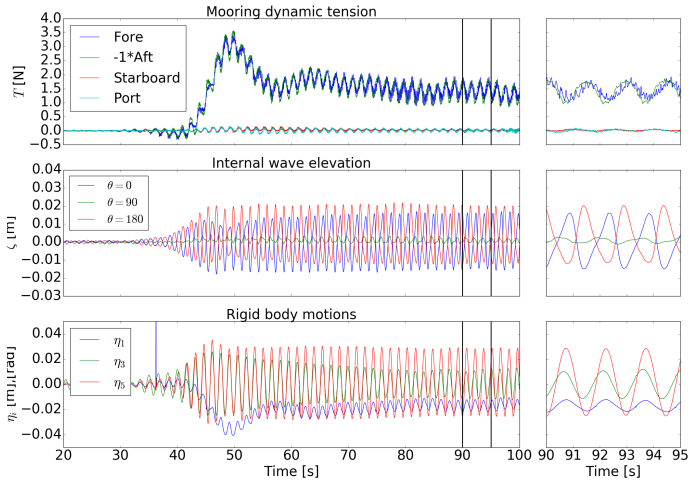

FIGURE 5: RAW TIME-SERIES OF MOORING LINE TENSION, INTERNAL WAVE ELEVATION AND RIGID BODY MOTIONS FROM SCALED MODEL TEST WITH THE WET MODEL IN REGULAR WAVES OF PERIOD $T = 1.50$ s AND STEEPNESS $H/\lambda = 1/45$.

RESULTS

The incident waves were documented by wave calibration tests for all wave conditions with no model present in the wavetank. The generated incident waves at the model location were found to be in agreement with the regular wave parameters input to the wavemaker for the major part of the test wave conditions. However, some deviations between the input wave height and the measured wave height were observed for the shortest wave periods. From decay tests with the wet model, the natural periods in surge, heave and pitch was found to be $T_{n1} = 11.4s$, $T_{n3} = 1.67s$ and $T_{n5} = 1.47s$, respectively. Correspondingly, natural periods for the dry model was found to be $T_{n1} = 13.7s$, $T_{n3} = 1.65s$ and $T_{n5} = 2.74s$. Typical time-series from the regular wave tests with the wet model are presented in Figs. 5 and 6.

Rigid Body Motions

Rigid body responses of the dry and wet model when subjected to regular waves were obtained from measured time-series of the scaled physical model tests. For each test, a time window was chosen from where steady state values of incident wave height and corresponding rigid body motion amplitudes were extracted. The resulting RAO's for surge, heave and pitch are presented in Figs. 7, 8, and 9, respectively, where the steady state motion amplitudes are normalized by the measured incident wave amplitude from the wave calibration tests. The effects of wave reflections from the side walls of the wave tank was investigated numerically with WAMIT. The presence of wall bound-

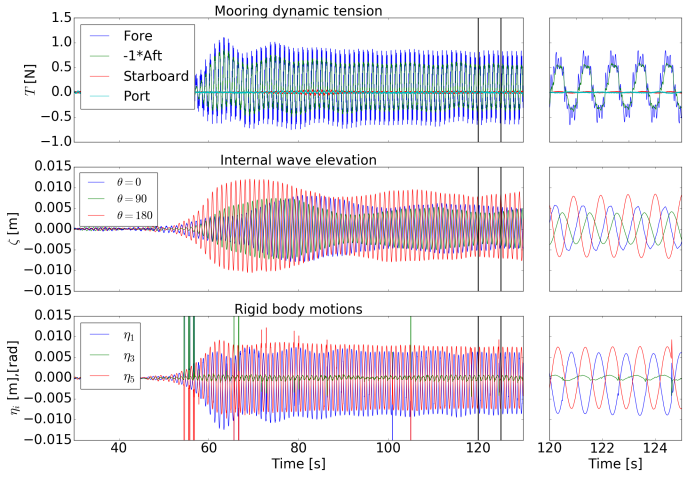

FIGURE 6: RAW TIME-SERIES OF MOORING LINE TENSION, INTERNAL WAVE ELEVATION AND RIGID BODY MOTIONS FROM SCALED MODEL TEST WITH THE WET MODEL IN REGULAR WAVES OF PERIOD $T = 1.04$ s AND STEEPNESS $H/\lambda = 1/60$.

aries was modeled by mirroring of the cage structure about the side walls of the wave tank. Four image bodies were applied to each side of the physical cage model in the simulation. The influence of wave reflection from the side walls on the RAO in heave obtained from simulations with WAMIT is presented in Fig. 10. The computed influence of wall effects on the surge and pitch modes of motion was small.

Mooring Forces

Measured time-series of tension in the mooring lines from the model experiments were analyzed to study mean wave drift forces. The net in-line horizontal force on the models was found by adding the time-series of measured tensions in the fore and aft mooring line. Similar as for analysis of the wave induced rigid body motions, a time window was found where the system was considered to have reached a steady state and the time-window was tapered using a Bingham window. A Butterworth digital low-pass filter of order 6 was applied with cut frequency $f_{cut} = 0.5/T$, where T is the wave period of the test considered. The first order dynamic tensions due to the wave-induced body motions were then removed and the mean force was found as the sample mean from the given time-window but with the tapered ends excluded. Negative values of the mean drift force was observed for the wet model for wave periods close to the natural period for the sloshing mode $f_{2,1}$. Numerical estimates of the mean wave drift force for the dry and wet models according to potential flow theory were obtained from WAMIT. To investigate

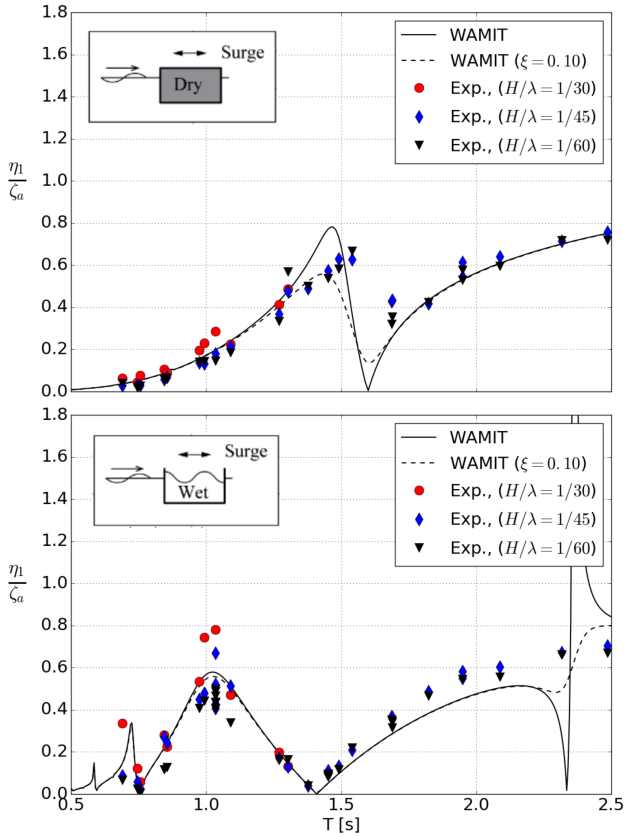

FIGURE 7: COMPARISON OF SURGE MOTIONS OBTAINED FROM SCALED MODEL TESTS WITH SURGE RAO'S FROM WAMIT. STIPPLED LINE IS RAO WITH ADDED DAMPING EQUAL TO 10% OF CRITICAL DAMPING.

the effect of damping on the mean drift force, simulations were performed where an additional damping force equal to 5 % of the critical damping was added to the potential damping. Figure 11 shows the mean wave-drift force for both the dry and wet model obtained from measurements as described above and compared with computed wave-drift force from WAMIT.

Sloshing

Induced responses of the contained water were measured as wave elevation at the inside wall of the model in a body fixed frame of reference. The linear harmonic component of the measured sloshing responses at different positions in the tank was obtained by band-pass filtering of the measured wave-elevation frequency spectrum around the incident wave frequency. A summary of the obtained results are presented in Fig. 12. Mean nonlinear wave amplitudes of sloshing at the front ($\xi_a^{(WP7)}$) and

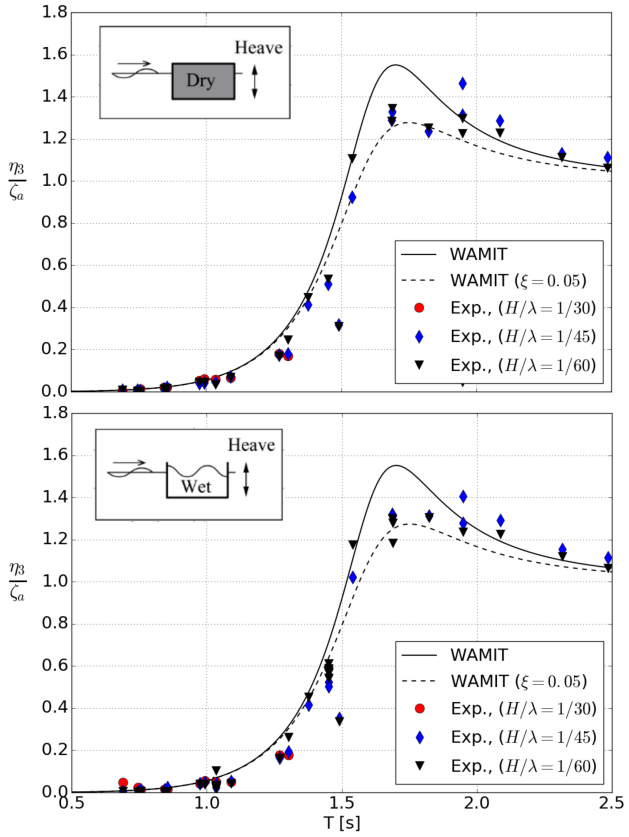

FIGURE 8: COMPARISON OF HEAVE MOTIONS OBTAINED FROM SCALED MODEL TESTS WITH HEAVE RAO'S FROM WAMIT. STIPPLED LINE IS RAO WITH ADDED DAMPING EQUAL TO 5% OF CRITICAL DAMPING.

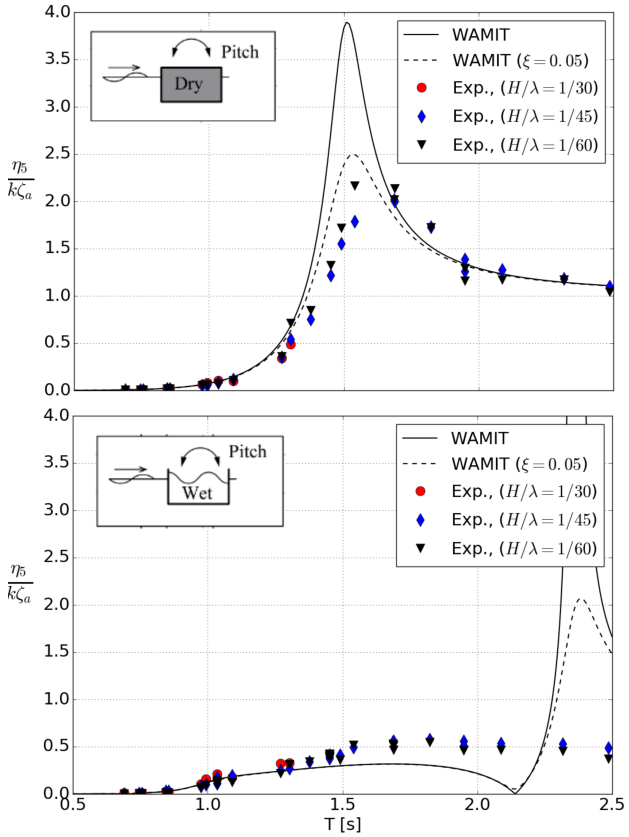

FIGURE 9: COMPARISON OF PITCH MOTIONS FROM SCALED MODEL TESTS WITH PITCH RAO'S FROM WAMIT. STIPPLED LINE IS RAO WITH ADDED DAMPING EQUAL TO 5% OF CRITICAL DAMPING.

aft ($\xi_a^{(WP11)}$) of the model are presented in Fig. 13. The sloshing amplitudes were normalized by the corresponding incident wave amplitudes. The standard deviation of the sloshing amplitudes also normalized by the corresponding incident wave amplitudes are plotted as error-bars. Large standard deviation is obtained where a steady state was not reached. Radiation forces (added mass and damping) for the surge, heave and pitch modes of motion were computed with WAMIT for both model configurations to investigate the effect of sloshing. Obtained frequency dependent added mass was found to be different for the two model configurations, while the obtained frequency dependent damping was found to be equal. Further, singularities were observed for the surge and pitch added masses at several frequencies, corresponding to natural frequencies of sloshing.

DISCUSSION

Rigid Body Motions

The RAO's in heave obtained from scaled model tests with the wet and the dry model configuration were almost identical (Fig. 8). This is consistent with linear potential flow theory, where there is no influence of sloshing on the coupled heave motion [6,11]. However, the heave RAO obtained from experiments had some deviations from the heave RAO resulting from WAMIT calculations. Deviations around the resonance period can be explained by viscous damping effects. Reflections of the radiated and diffracted waves from the side-walls of the wave tank was also found to influence the heave motion in the experiments. Influence of wall reflections on the heave motion was also found from WAMIT (Fig. 10). Comparison of obtained RAO's from experiments and numerical simulations shows large impact of sloshing on the surge and pitch modes of motion (Figs. 7 and 9). The pitch motion amplitudes of the wet model are largely reduced compared to that of the dry model around the pitch reso-

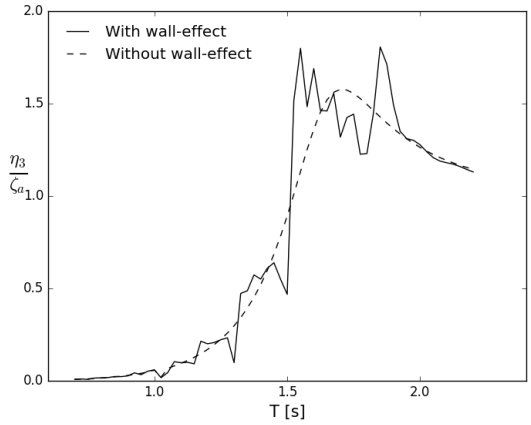

FIGURE 10: EFFECT OF WAVE REFLECTION FROM TANK WALLS ON THE HEAVE RAO OBTAINED FROM NUMERICAL SIMULATIONS WITH WAMIT.

nance frequency for the dry configuration, as the presence of the internal free surface has a destabilizing effect that increases the pitch natural period. For the wet model configuration, large deviations were observed between the computed and measured pitch motions. This is assumed to be caused by a difference in the pitch natural period predicted by WAMIT ($T_{n5}^{(num)} = 2.38$ s) relative to that obtained from experiments ($T_{n5}^{(exp)} = 2.74$ s). Due to coupling effects, this also results in deviations between the computed and measured motions in surge for the wet model for wave periods around $T = 2.38$ s. Comparison of numerically obtained surge responses for the wet and dry model configuration (Fig. 7) shows that sloshing results in 200 % amplification of the surge motion amplitudes for wave periods around the natural sloshing period $T_{2,1}$. Measured surge response for the dry and wet model configuration shows similar comparison, but where a nonlinear amplification in surge is observed for the wet model for wave periods around $T_{2,1}$. These wave periods can be relevant for typical fjord locations for scale factors of medium sized closed cages. The identified nonlinear behavior could not be captured by the present linear numerical analysis, and a nonlinear multi-modal method for the internal sloshing as presented in [6] is suggested to improve the results.

Sloshing

In a linear seakeeping analysis, the effect of sloshing is a modified added mass matrix [11]. The potential damping matrix is not affected by the sloshing, as potential damping is associated with energy loss due to wave radiation. In the present numerical study, the computed added mass in surge and pitch were found to be singular for periods corresponding to natural periods of the antisymmetric sloshing modes $f_{1,1}$, $f_{1,2}$ and $f_{1,3}$, which is

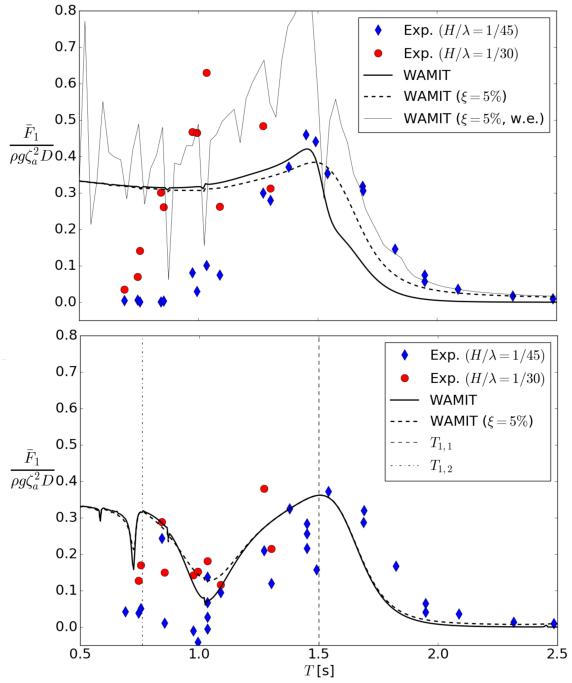

FIGURE 11: COMPARISON OF MEAN WAVE DRIFT FORCE FOR THE DRY MODEL (TOP) AND WET MODEL (BOTTOM) OBTAINED FROM MODEL TESTS AND FROM WAMIT. WAMIT RESULTS ARE WITH AND WITHOUT ADDED DAMPING AND WITH WALL EFFECTS (DRY MODEL ONLY). THE TWO LOWEST NATURAL PERIODS OF SLOSHING WITH FORE-AFT ASYMMETRY IS PLOTTED AS VERTICAL LINES.

consistent with [11]. The linear harmonic sloshing amplitudes from experiments normalized by the incident wave amplitude, presented in Fig. 12, shows that largest amplification of sloshing occur for incident wave periods 0.76 s and 1.04s for most of the wave probes. These periods are close to the natural sloshing periods $T_{1,2}$, $T_{4,1}$ and $T_{2,1}$, where also nonlinear behavior of sloshing are observed as seen in Fig. 13. Although $T_{2,1}$ corresponds to the symmetric sloshing mode $f_{2,1}$ (see Fig. 3), the measured wave elevation inside the tank at the front and aft side is found to be approximately 180° out of phase, which indicates the presence of antisymmetric modes. Steady state sloshing amplitudes were not obtained for the tests with incident wave period 1.04 s, where a beating phenomenon was observed as shown in Fig. 6. This might be due to nonlinear effects of sloshing [6]. Further, this corresponds to the wave period where the nonlinear amplification of the surge motion with increasing wave steepness was observed (Fig. 7). The importance of the nonlinearity of sloshing on coupling effects with ship motions was emphasized by [10].

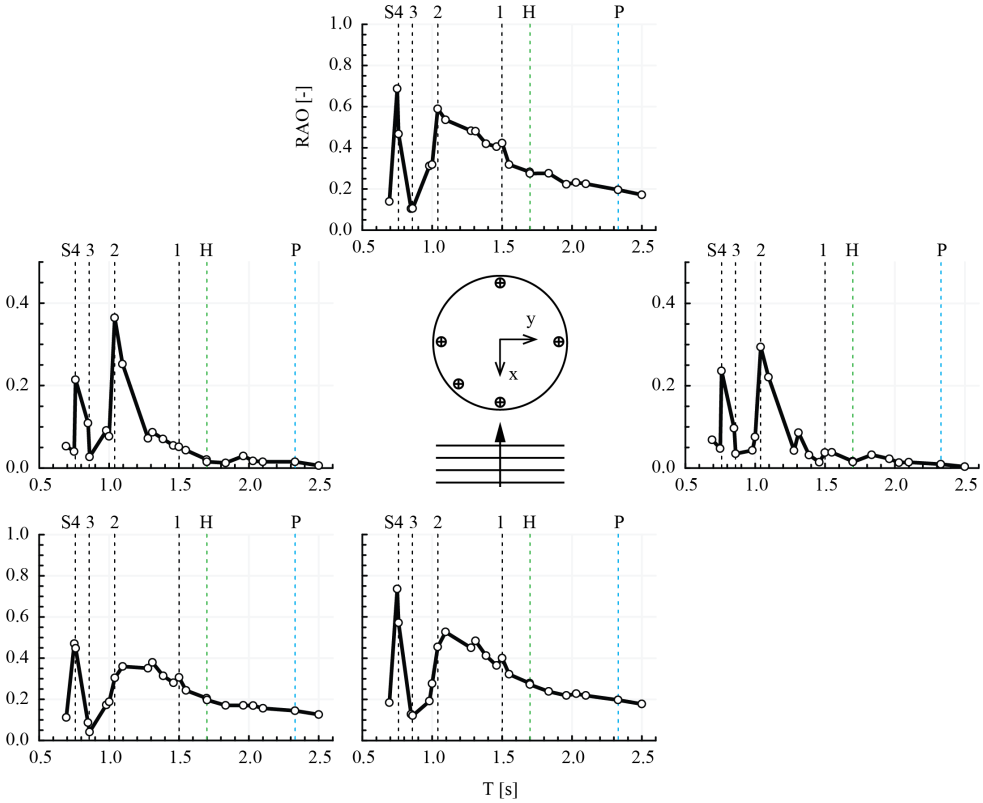

FIGURE 12: SLOSHING AMPLITUDES FROM EXPERIMENTS AT FIVE DIFFERENT LOCATIONS INSIDE THE CLOSED CAGE FROM TESTS WITH $H/\lambda = 1/45$. WAVE ELEVATION IS GIVEN IN A BODY FIXED FRAME OF REFERENCE. HEAVE (H) AND PITCH (P) NATURAL PERIODS AND THE FOUR HIGHEST NATURAL PERIODS OF SLOSHING (S1-4) ARE INDICATED BY VERTICAL STIPPLED LINES.

Mooring Forces

As the mooring forces are directly influenced by the first order surge motions, from the above discussion it is clear that effects of sloshing can be important for the mooring forces. Comparison of the mean drift force obtained from measured time-series of mooring line tensions in the scaled model tests with the dry and wet model presented in Fig. 11, shows that the wave drift force is influenced by sloshing (see also Figs. 5 and 6). This is reasonable as the wave induced motions have impact on the mean wave loads [16]. The influence of sloshing on the mean wave loads was also demonstrated by Newman [11]. Large deviation between experiments and numerical results are observed for the wave drift force for the lower wave periods for both model configurations. The deviation for the dry model cannot be explained by sloshing, but wave reflections from the side walls are found to have large influence on the mean wave drift force. Large scatter is observed of the wave drift force from experiments with the wet model in particular for wave periods around the sloshing period $T_{2,1}$, where even negative values of the wave drift force were observed. Other effects that could have influenced the mean drift force were friction in the pulleys of the mooring system, precision of the load cells when measuring small quantities, or nonlinear hydrodynamic effects due to water exit and entry of the slender floating collar in waves (cf. Fig. 1).

Possible Errors In Experiments

The uncertainties identified in the present experiments not already discussed, are presented in the following. Repetition tests were performed for several test conditions to quantify precision errors. Some variations in the repetition tests were observed for the test wave periods around the natural periods of sloshing. Possible sources to bias errors are related to the wave kinematics for the shortest wave periods. Irregularities were observed due to instabilities of the wave crests after many wave lengths of propagation. Further, the filling level of water inside the model was controlled visually, based on the equilibrium water line, yielding an expected uncertainty of the order ± 5 mm.

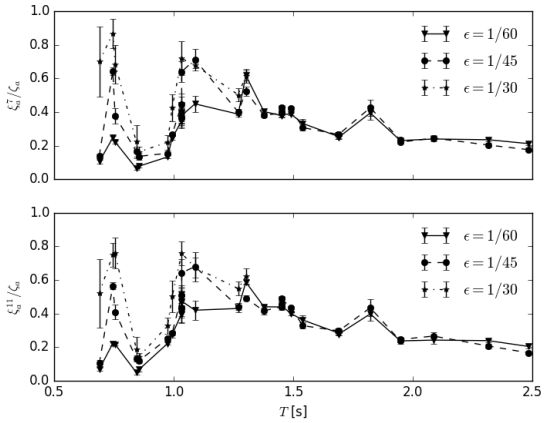

FIGURE 13: MEAN NONLINEAR SLOSHING AMPLITUDES FROM MODEL TESTS NORMALIZED BY INCIDENT WAVE AMPLITUDE. UPPER: WAVE AMPLITUDE AT FRONT ($\theta = 0$). LOWER: WAVE AMPLITUDE AT AFT ($\theta = 180°$). NORMALIZED STANDARD DEVIATION IS SHOWN AS ERROR BARS.

CONCLUSION

In the present paper, a study of the seakeeping behavior of a floating closed cage structure was presented, including scaled model tests and numerical calculations with WAMIT. Special attention was drawn to the coupling effects of sloshing on the wave induced rigid body motions of the closed cage. Comparison of results showed that sloshing of the contained water has large influence on the coupled surge and pitch modes of motion. A nonlinear effect of wave steepness on the surge motion was observed for incident wave periods around the natural period of sloshing corresponding to mode shape $f_{2,1}$, where the surge motion increased with increasing wave steepness. This could not be captured by a linear analysis, and a nonlinear multi-modal method of sloshing is suggested to improve the predictions. Large deviations were observed between mean wave drift force obtained from simulations and mean mooring force from model experiments. However, still sloshing was found to have significant effect on the mean wave drift force. Hence, it is important to consider sloshing and associated coupling effects in design of closed fish cages and their mooring systems.

ACKNOWLEDGMENT

This work was funded by the Norwegian Fisheries and Aquaculture Research Fund (FHF) through grant no. 901287 and the Norwegian Research Council's MAROFF program through grant no. 268402.

REFERENCES

[1] Solaas, F., Rudi, H., Berg, A., and Tvinnereim, K., 1993. "Floating fish farms with bag pens". In Fish Farming Technology.

[2] Løland, G., and Aarsnes, J. V., 1994. "Fabric as construction material for marine applications". In Hydroelasticity in Marine Technology, pp. 275–286.

[3] Lader, P., Fredriksson, D. W., Volent, Z., DeCew, J., Rosten, T., and Strand, I., 2015. "Drag forces on, and deformation of, closed flexible bags". *Journal of Offshore Mechanics and Arctic Engineering,* ***137***(4), pp. 041202–041202–8.

[4] Strand, I., Sørensen, A., Volent, Z., and Lader, P., 2016. "Experimental study of current forces and deformations on a half ellipsoidal closed flexible fish cage". *Journal of Fluids and Structures,* ***65***(Supplement C), pp. 108 – 120.

[5] Lader, P., Fredriksson, D. W., Volent, Z., DeCew, J., Rosten, T., and Strand, I., 2017. "Wave response of closed flexible bags". *Journal of Offshore Mechanics and Arctic Engineering,* ***139***(5), pp. 051301–051301–9.

[6] Faltinsen, O. M., and Timokha, A. N., 2014. *Sloshing*. Cambridge University Press.

[7] Rognebakke, O. F., and Faltinsen, O. M., 2001. "The effect of sloshing on ship motions". In 16th International Workshop on Water Waves and Floating Bodies.

[8] Faltinsen, O. M., and Timokha, A. N., 2001. "An adaptive multimodal approach to nonlinear sloshing in a rectangular tank". *Journal of Fluid Mechanics,* ***432***, p. 167200.

[9] Rognebakke, O. F., and Faltinsen, O. M., 2003. "Coupling of sloshing and ship motions". *Journal of Ship Research,* ***47***(3), Sept., pp. 208–221.

[10] Kim, Y., Nam, B., Kim, D., and Kim, Y., 2007. "Study on coupling effects of ship motion and sloshing". *Ocean Engineering,* ***34***(16), pp. 2176 – 2187.

[11] Newman, J. N., 2005. "Wave effects on vessels with internal tanks". In 20th International Workshop on Water Waves and Floating Bodies.

[12] Malenica, S., Zalar, M., and Chen, X. B., 2003. "Dynamic coupling of seakeeping and sloshing". In Proceedings of The Thirteenth (2003) International Offshore and Polar Engineering Conference.

[13] Newland, D., 1984. *An introduction to random vibrations and spectral analysis*. Longman.

[14] Davies, L., and Gather, U., 1993. "The identification of multiple outliers". *Journal of the American Statistical Association,* ***88***(423), pp. 782–792.

[15] WAMIT, INCORPORATED AND MASSACHUSETTS INSTITUTE OF TECHNOLOGY, 2013. *WAMIT User Manual Version 7.0*, version 7.062 ed. WAMIT, Inc., 822 Boylston St. - Suite 202, Chestnut Hill, MA 02467-2504, USA, Oct.

[16] Faltinsen, O., 1993. *Sea Loads on Ships and Offshore Structures*. Cambridge Ocean Technology Series. Cambridge University Press.